Wear 478-479 (2021) 203758

Contents lists available at ScienceDirect

Wear

journal homepage: http://www.elsevier.com/locate/wear

Orientation dependence of the wear resistance in the Co–Cr–Mo single crystal

Takayoshi Nakano [a,*,#], Koji Hagihara [a,#], Ana R. Ribeiro [b,c,1], Yusuke Fujii [a], Tsubasa Todo [a], Ryo Fukushima [a], Luís Augusto Rocha [c,d]

[a] Division of Materials and Manufacturing Science, Graduate School of Engineering, Osaka University, 2-1 Yamadaoka, Suita, Osaka, 565-0871, Japan
[b] Postgraduate Program in Biotechnology, National Institute of Metrology Quality and Technology, Rio de Janeiro, Brazil
[c] IBTN/Br–Brazilian Branch of the Institute of Biomaterials, Tribocorrosion and Nanomedicine, Universidade Estadual Paulista–UNESP, Av. Eng. Luiz Edmundo Carrijo Coube, Bauru, 17033-360, São Paulo, Brazil
[d] Faculdade de Ciências, Departamento de Física, Universidade Estadual Paulista–UNESP, Av. Eng. Luiz Edmundo Carrijo Coube, Bauru, 17033-360, São Paulo, Brazil

ARTICLE INFO

Keywords:
Co–Cr alloy
Wear
Single crystal
Biomaterial
Hardness
Orientation dependence

ABSTRACT

This is the report clarifying the orientation dependence of the wear behavior of Co–Cr–Mo alloy. The wear resistance of the Co–Cr–Mo alloy with face-centered cubic (fcc) structure was found to be higher on the planes in order of {110}, {001} and {111}. Quantitatively, the wear resistance on {110} is 1.5 times larger than that on {111}. The tendency showed in coincident with the orientation dependence of the surface hardness, as empirically suggested. However, we additionally found in the observation of the worn surface in the fcc-single crystals that the volume fraction of the hexagonal close-packed (hcp)-phase, which was formed as the strain-induced martensite during the wear test, was larger in the same order of the wear resistance. The variation in formation frequency of the hcp-phase during the wear test can be explained by focusing on the Schmid factor along the resultant direction of the applied stress and the friction stress. On the {111} surface where the Schmid factor for the strain-induced ε-martensite formation is small, homogeneous deformation microstructure covered by it was not developed even after long-time wear, resulting in lower wear resistance. The results strongly suggest that not only the hardness, but the distribution of the ε-martensite is important to control the wear behavior of the Co–Cr alloys with the extremely low stacking fault energy, and it can be achieved by the crystal orientation control in the γ-phase.

1. Introduction

Co–Cr–Mo alloys have been widely applied as heat-resistance materials. In addition, its Ni-free alloys are particularly used for surgical implants owing to their high strength, high corrosion resistance, and modest biocompatibility [1–3]. Especially, owing to its superior wear behavior, the Co–Cr–Mo alloys are widely used in hip and knee hip joint prostheses. In these applications, in which sliding between surfaces occurs, the control or minimization of wear degradation is essentially required, since the interactions of metal particles and ions with cells, as a result of the prolonged wear, are mostly harmful for patients [4,5]. In fact, in the clinical practice, debris with the same chemical composition of the prosthesis have been detected in the synovial fluid and capsule, in liver and kidneys of patients leading to cases of inflammation, metallosis, pseudotumors and consequent prostheses failure [6–8]. To reduce wear, Co–Cr–Mo alloys are often used as a combination with the ultra-high molecular weight polyethylene (UHMWPE) [9]. The wear coefficients of Co–Cr–Mo alloys are among the lowest when sliding against UHMPWE counterfaces. However, for the further improvement of wear properties, fundamental understanding of the wear properties of the Co–Cr–Mo alloy itself is essentially required for its control.

There are many reports on the mechanical properties (deformation behavior [10–16], wear behavior [17–26] etc.) of Co–Cr–Mo alloys in the polycrystalline form. However, fundamental knowledge on the effect of the crystal structure and orientation on the mechanical properties of Co–Cr–Mo alloys is needed in order to provide new strategies to improve

* Corresponding author.
E-mail address: nakano@mat.eng.osaka-u.ac.jp (T. Nakano).
# The authors equally contributed to this study: Takayoshi Nakano, Koji Hagihara.
[1] Biomaterials, Biodegradables and Biomimetics Research Institute (I3Bs), University of Minho, 4800–058, Guimarães, Portugal.

https://doi.org/10.1016/j.wear.2021.203758
Received 22 November 2020; Received in revised form 23 February 2021; Accepted 24 February 2021
Available online 11 March 2021

those properties. Thus in last year's our group is studying Co–Cr–Mo single crystals [27,28]. The cast Co–Cr–Mo alloys are usually composed of an fcc-phase [2], although the fcc-phase is the stable phase at high-temperature [29]. When the stress was applied to the fcc-phase alloy at room temperature, the plastic deformation predominately proceeds by a strain-induced martensitic transformation (SIM) from the γ(fcc)-phase to the ε(hcp)-phase which is the low-temperature stable phase. We recently clarified that the plastic deformation behavior of the Co–Cr–Mo alloys shows the strong orientation dependence, and the variation is more enhanced by the control of the microstructure [27]. Such variation in deformation behavior with loading orientation is expected to affect the wear behavior also, but there is no report on it until now. Furthermore, there are few studies to clarify the crystal orientation dependence of wear behavior using the single crystal, not only in Co–Cr–Mo alloys but also in other metallic materials [30–33]. Thus, to obtain the information on this is important.

In addition, we have recently proposed the development of "single-crystal implant materials" in β-Ti alloys [34–38], which allows the superior characteristics of metallic biomaterials to be fully attained by controlling the crystal orientation. It is strongly expected that a similar strategy must be applicable to Co–Cr–Mo alloys. Thus, the study of single crystals is essential to further development of Co–Cr–Mo alloys for biomedical implant applications.

According to these backgrounds, orientation dependence of the wear behavior of the Co–Cr–Mo alloys was examined in this study. The controlling factors that affect the orientation dependence of the wear behavior are discussed.

2. Experimental procedure

A mother ingot with a composition of Co–27Cr–6Mo (wt.%), as defined by ASTM F75-18, was supplied by Teijin Nakashima Medical Co. Ltd., Japan. Using the mother ingot, single crystals were grown by the Bridgman method at a growth rate of 5 mm/h in an Ar atmosphere in an Al_2O_3 crucible, as shown in Fig. 1. The alloy compositions (mass%) in the mother ingot and obtained single crystal were measured, and the results were listed in Table 1. The alloy composition showed almost no change before and after the single crystalline growth. Only the amount of Al was slightly increased, which is owing to the reaction with Al_2O_3 crucible [27].

By the X-ray Laue back diffraction method, the successive growth of γ-phase single crystals was confirmed. The detailed feature for the preparation method and the microstructure in the single crystal are referred to in our previous paper [27]. As a notable feature of the microstructure, Fig. 2(a) shows the bright field image observed by the transmission electron microscopy (TEM, JEOL JEM-3010), and Fig. 2(b, c) show the crystal orientation maps taken by the electron back-scatter diffraction pattern analysis in the scanning electron microscopy (SEM-EBSD, SEM: JEOL JSM-6500F, EBSD: TSL solutions) in the obtained single crystal for γ(fcc) and ε(hcp)-phases, respectively. As reported in Ref. [27], the obtained single crystal contains small amount of thin stacking-fault-like ε-phases only on the specific one of four {111} planes, different from the feature generally observed in the annealed polycrystals as described later in details. We define the plane on which thin stacking-fault-like ε-phases exist as the (111) plane in the obtained single crystal. No other precipitates such as Al_2O_3 and σ-phase were observed in the single crystal. The details of the microstructure were previously reported in Ref. [27].

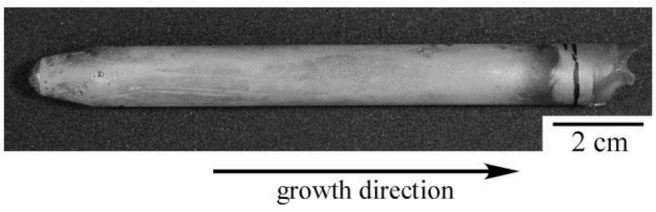

Fig. 1. Appearance of the Co–Cr–Mo single crystal grown by the Bridgman method.

Prior to the wear test, orientation dependence of the Vickers hardness was examined to discuss the relation between the hardness and wear behavior. The hardness tests were conducted on the (001), (110) and (111) planes at a load of 500 gf.

The wear behavior of the Co–Cr–Mo alloy single crystal was evaluated by the conventional pin-on-disc type wear test (Rhesca FPR2100, Japan). From the obtained single crystal, the pins with the diameter of 2 mm and the length of 7 mm were cut out by the electro-discharge machining (EDM). Three different loading orientations were selected in the preparation of single crystalline pins, as the longitudinal direction of the pin is aligned parallel to [001], [110] and [111] within an error of 1°, and the orientation dependence of the wear behavior was examined. As the counterbody of single crystalline pin, the disc specimen with a diameter of 20 mm and 4 mm in thickness was prepared using the cast Co–Cr–Mo alloy polycrystalline ingot by EDM. By the X-ray diffraction analysis, it was confirmed that the cast Co–Cr–Mo alloy was mainly composed of γ-phase, but ε-phases was also present with a fraction of ~30%. No other precipitates were observed in the cast alloy. Further, by the SEM-EBSD analysis, the average grain size of the γ-matrix phase in the polycrystalline disc was evaluated to be ~800 μm, and no significant texture was developed in it.

In addition, some pins with [111] loading orientation were heat-treatment at 800 °C for 40 h prior to the wear test to transform the crystal structure from γ to ε, and the influence of the variation in crystal structure to the wear behavior was also examined. The surface of the specimen was mechanically polished with emery paper and final polishing was conducted used by the colloidal silica to ensure the surface roughness, R_a, smaller than 0.05 μm. The ε-SIM formation during the preparing and polishing processes of the specimens were prevented by the careful treatment, and no introduction of ε-SIM was confirmed by the surface observation before the test.

The wear test was conducted in a dry condition; the humidity and temperature were kept at 30% and 20 °C during the test. The applied load for the pin was 9.8 N. The pin was set at the position of 8 mm from the center of the disc, and the disc was rotated at 24 rpm, resulting in a relative sliding speed of 20 mm/s. Note that in the determination of the crystal orientation of the single crystalline pins, not only the parallel direction (loading orientation) of the pin, crystal orientations of two other perpendicular directions with respect to the loading direction, one of which is always parallel to $[1\bar{1}0]$, were determined and marked. Then, by setting the $[1\bar{1}0]$ parallel to the tangent direction of the wear circle, the shear direction of the pin with respect to the disc was commonly set to be parallel to $[1\bar{1}0]$ in all the specimens investigated. The single crystalline pin was fixed by sandwiching with two screws in the holder to precisely locking the crystal orientation in the tests. The wear test lasted for 1 week; the total wear sliding distance is ~12.15 km. Variations in masses of the pin and disk during the test were measured every 6 h using an electronic balance, and by comparing them with the initial masses, the wear mass loss was evaluated. Then, the wear volume was evaluated by dividing the wear mass loss value by the alloy density (8.40 g/cm^3). The variations in coefficient of friction during the test was evaluated by dividing the measured friction stress by the applied load (9.8 N). The wear test was conducted twice at each condition, to check the reproductivity of the result.

After the test, the worn surface and wear debris were examined in the SEM to assist the analysis of wear mechanisms. The variations in surface roughness on the pin and disk after the test were evaluated via the observation using laser microscope. In addition, the variation in microstructure with crystal orientation induced by the wear test was examined by SEM-EBSD and TEM.

Table 1
The alloy compositions (mass%) in the mother ingot and obtained single crystal.

	Chemical composition (mass%)								
	Cr	Mo	N	Ni	Fe	Al	C	Si	Co
ASTM F75-18	27.00–30.00	5.00–7.00	<0.25	<0.50	<0.75	<0.10	<0.35	<1.00	Bal.
Mother ingot	27.13	5.87	0.04	0.03	0.10	<0.001	0.01	0.57	Bal.
Single crystal	27.10	5.67	0.03	0.03	0.06	0.18	0.034	0.58	Bal.

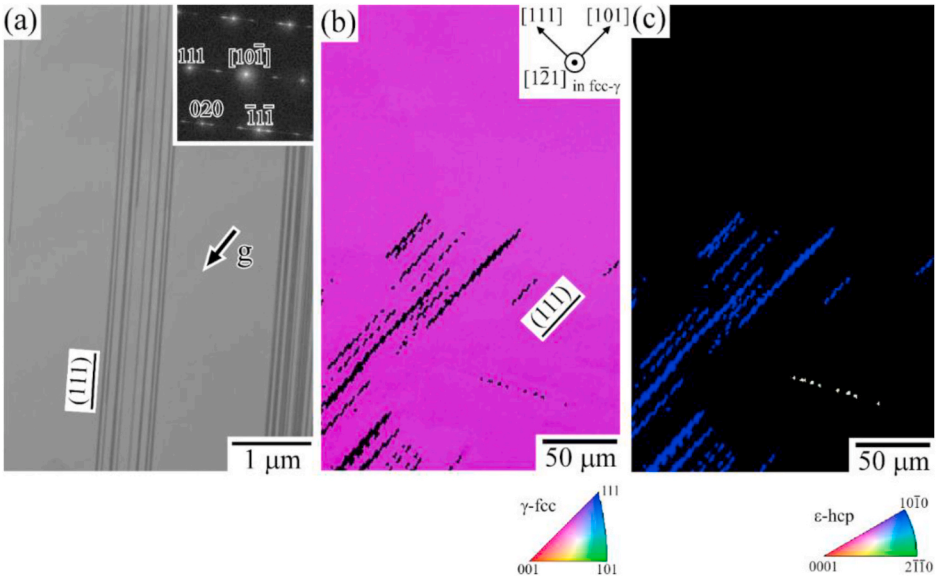

Fig. 2. Microstructure in the obtained Co–Cr–Mo single crystal. (a) TEM bright field image observed along $[10\bar{1}]$. (b, c) Crystal orientation maps taken by SEM-EBSD for (b) γ(fcc)-phase and (c) ε(hcp)-phase, measured along $[1\bar{2}1]_\gamma$.

3. Results

Fig. 3 shows the relation between the wear volume of the single crystalline Co–Cr–Mo pin and the sliding distance in the wear tests, as a function of loading orientation and heat-treatment. The wear volume monotonically increased with the sliding distance in all the tested specimens, but the detailed behavior was slightly different in them. The wear volume was almost proportionally increased with the sliding distance throughout the test in (001) and (111) specimens, while the wear rate was slightly deceased at the latter period of the wear test in the (110) specimen. In addition, the absolute value of the wear volume measured by the 1 week of wear test showed significant differences depending on the loading orientation. The wear volume was higher for the specimens whose wear plane was parallel to (111), followed by the (001) and (110), respectively. Surprisingly, the wear volume of (110) specimen was more than 30% smaller than that observed in the (111) specimen, even if they have completely the same composition.

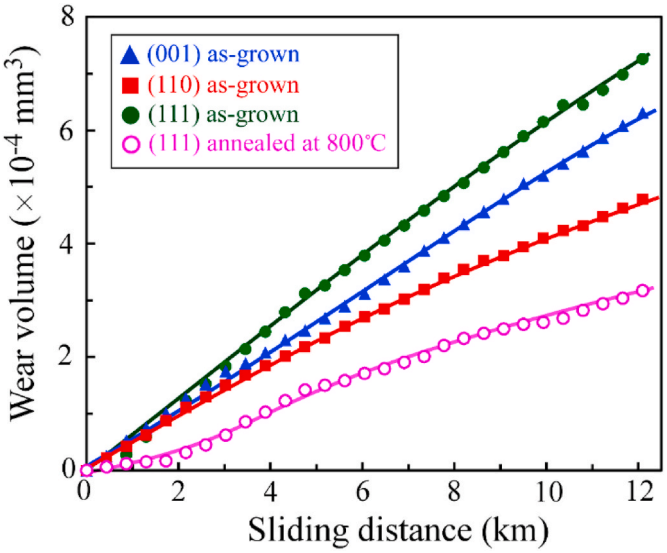

Fig. 3. Variations in wear volume of the single crystalline Co–Cr–Mo pin during the wear test, as a function of loading orientation and heat-treatment.

In addition, the heat-treatment drastically influenced the wear resistance. Even though the wear volume of the (111) specimen was the largest in the as-grown condition, the value became less than half by the heat-treatment at 800 °C for 40 h, and then the wear volume showed a more than 30% smaller value than that at (110) measured in the as-grown state.

Fig. 4 shows the variations in the wear volume of the polycrystalline Co–Cr–Mo disk as the counterbody of the single crystalline pin during the wear test. The order of the amount of wear volume of the disk showed the opposite trend compared to that of the single crystalline pin shown in Fig. 3, although the difference was small in case that the pins are the γ-phase single crystal.

To clarify the origin for the variation in wear volume with crystal orientation, controlling mechanism of the wear behavior in the Co–Cr–Mo single crystal was examined. Fig. 5 presents the SEM images showing the appearance of the surface of the pins after the wear test for 1 week. The worn surfaces showed the typical characteristics of abrasive wear and adhesive wear, indicated by the presence of significant grooves and small damages by third-body abrasive particles in all the specimens, and no significant difference depending on the crystal orientation was confirmed. The grooves were introduced homogeneously in the entire specimen surface with the average depth of 2–3 μm and with the width

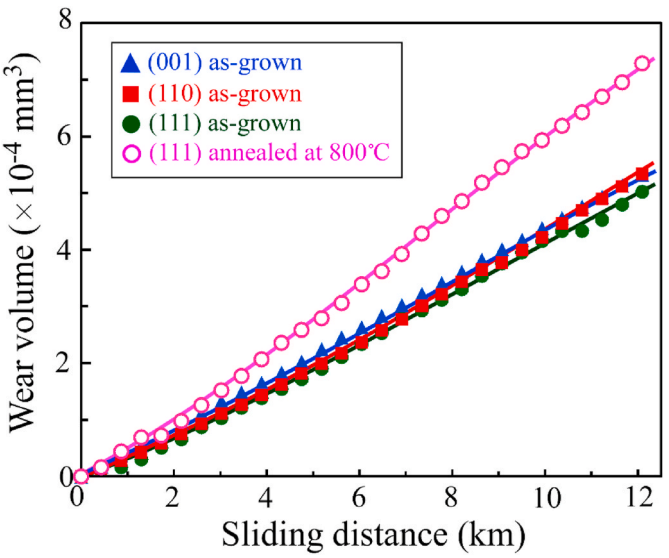

Fig. 4. Variations in the wear volume of the polycrystalline Co–Cr–Mo disk as the counterbody of the single crystalline pin shown in Fig. 3, during the wear test.

of 15–20 μm in all the specimens. The geometry of the shape of groove was carefully examined by using laser microscopy, but the crystallographic relationship with respect to its shape, i.e. formation of faceted surface along a specific crystallographic plane on the surface of the groove was not confirmed.

Fig. 6 shows the quantitative evaluation results of the surface roughness on the worn pin and disk. No significant difference in surface roughness was confirmed in the γ-phase single crystalline pins; R_a of ~0.5 μm was measured in the specimens. The surface roughness was larger than that measured on the worn disk (R_a = ~0.4 μm), demonstrating that deeper grooves were formed on the pin by the abrasive wear in the γ-phase single crystals. On the other hand, in the annealed (111) pin, i.e. the pin is composed of ε-phase as proved later, the surface roughness on the pin was smaller than that on the disk.

Fig. 7 shows the variation in specific wear rate, ω, as a function of sliding distance during the wear test. The value of ω was evaluated from the data shown in Fig. 3 by the following equation:

$$\omega = \frac{W_1 - W_2}{P \cdot L \cdot \rho} \quad (1)$$

where, W_1 and W_2 are the weight of the pin before and after the wear test, P the applied load, L the sliding distance, ρ the density of the Co–Cr–Mo single crystal. Thus, ω indicates the variation in wear volume per unit sliding distance and load during the wear test. Although the ω value showed a slight orientation dependence, the values all existed in the range between 10^{-7} and 10^{-8} throughout the wear test. It has been reported that the value of specific wear rate varies depending on the wear mechanism [20,39]. The obtained ω value in this study is similar to that reported by Kumagai et al. in a forged Co–Co–Mo alloy, in which

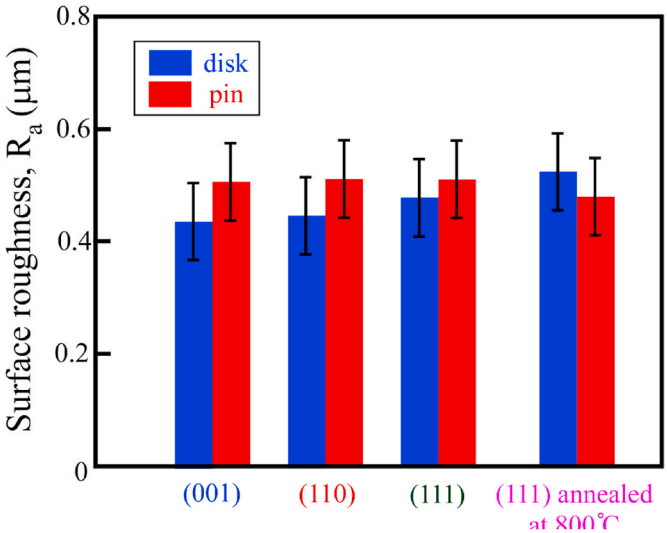

Fig. 6. Surface roughness on the worn single crystalline pins and polycrystalline disks after the wear test.

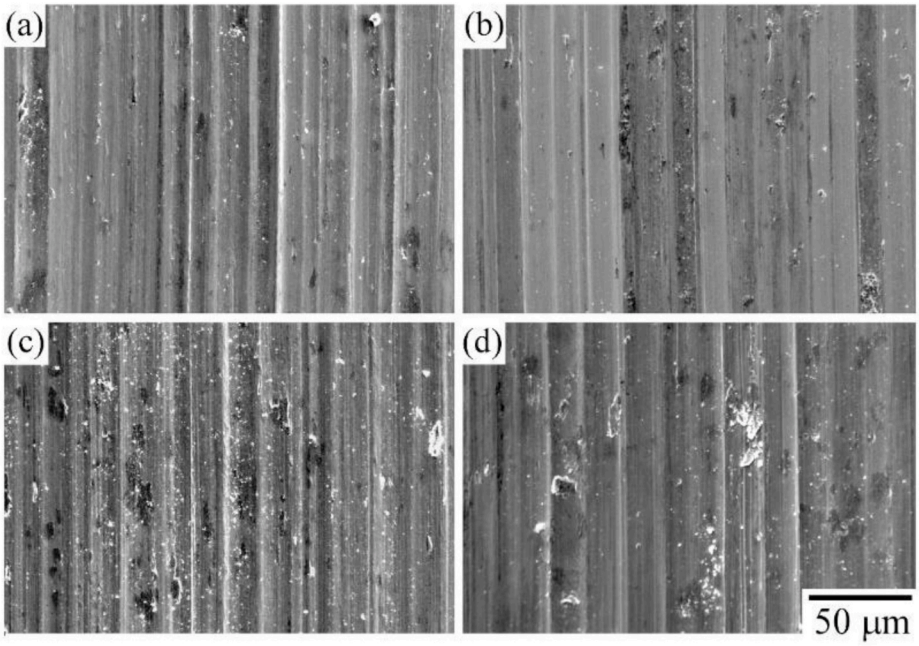

Fig. 5. Surface morphologies of the single crystalline pins after the wear test. Surface normal is parallel to (a) [001], (b) [110] and (c) [111], respectively. (d) [111] specimen annealed at 800 °C for 40 h prior to the wear test.

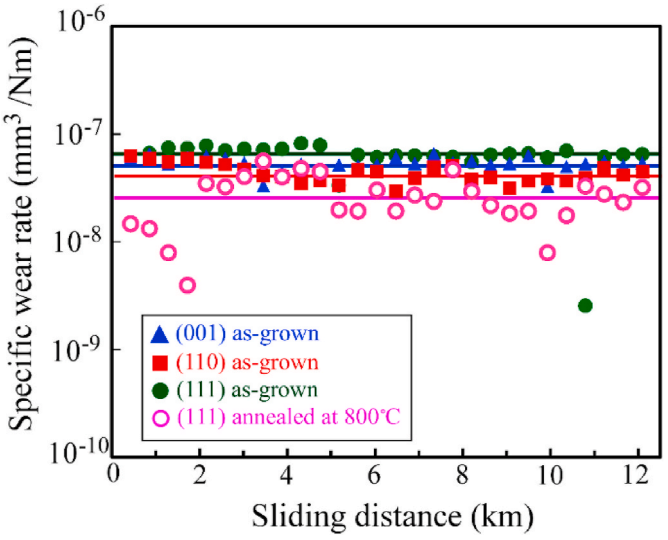

Fig. 7. Variation in the specific wear rate, ω, as a function of sliding distance during the wear test.

both an abrasive wear and adhesive wear occurred [20]. Combined with the observation results of the worn surface shown in Fig. 5, it is suggested that the wear of the Co–Cr–Mo single crystals predominately occurred by the abrasive wear mechanism independent of the crystal orientation and heat treatment, and no significant change in wear mechanism occurred during the wear test conducted. That is, the experimental results demonstrate that although the absolute value of wear volume was largely varied, the wear mechanism itself does not vary depending on the crystal orientation and heat treatment.

Fig. 8 shows the variation in coefficient of friction measured during the wear test. The coefficient of friction showed an almost constant value of 0.44–0.46 in all the specimens throughout the test. This result also suggests that the same wear mechanism governs the wear behavior of the Co–Cr–Mo single crystals independent of the crystal orientation.

It is empirically suggested that the wear resistance is related to the surface hardness of the material, and the following relationship is proposed [40,41].

$$V = K \cdot \frac{P}{H} \cdot L \tag{2}$$

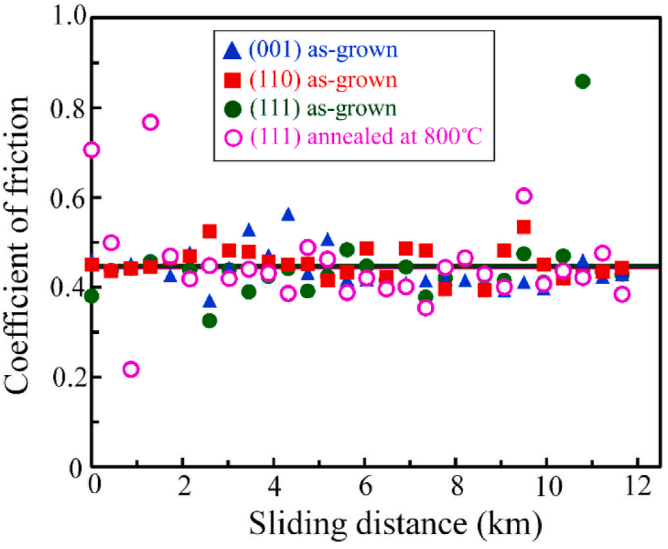

Fig. 8. Variation in coefficient of friction, μ, as a function of sliding distance during the wear test.

where V is the wear volume, P the applied load, H the hardness, L the sliding distance, and K the constant. To clarify the origin of the orientation dependence of the wear behavior of the Co–Cr–Mo single crystal, the orientation dependence of the hardness was examined by the Vickers hardness, as the result is shown in Fig. 9(a). As well as the wear volume, the hardness showed a significant orientation relationship, and it showed higher values in order of (111) < (100) < (110) in the as-grown crystal. In addition, the hardness was largely increased by the heat treatment, and the hardness of the annealed (111) crystal was higher compared to all of the as-grown crystals. Fig. 9(b) presents the relation between the wear volume and the inverse of the Vickers hardness obtained in the single crystals. The increase in hardness, i.e. the decrease of the inverse of the hardness, decreased the wear volume, demonstrating that the "empirical low" is applicable also for the single crystal. However, it is to note that their relations are slightly deviated from the proportional relationship anticipated by equ. (2). This suggests that although the surface hardness is indeed one of the important factors which control the wear behavior of the Co–Cr–Mo crystal, other factors which affect the orientation dependence of wear behavior must exist. The details on this is discussed in section 4.2.

As shown in Fig. 9(a), the hardness was largely increased by the heat-treatment. To clarify the detailed reason of this, the variation in

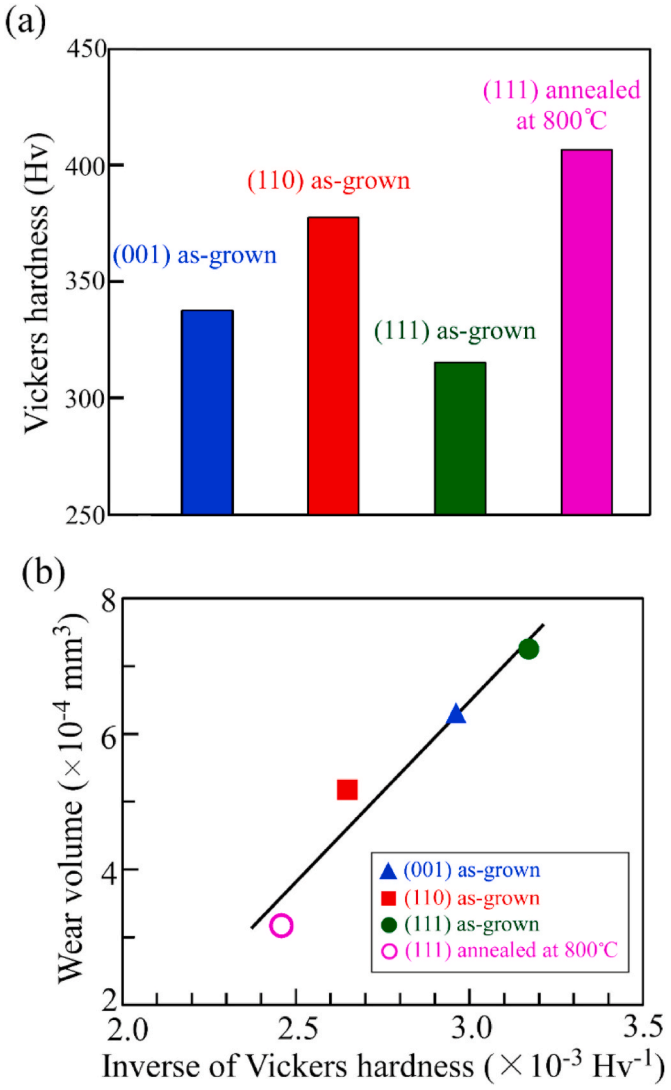

Fig. 9. (a) Orientation dependence of the hardness in the Co–Cr–Mo single crystal measured by the Vickers hardness test. (b) Relation between the wear volume and the inverse of the hardness.

microstructure was examined by the SEM-EBSD analysis. Fig. 10(a, b) show the crystal orientation maps taken in the heat-treated crystal. As shown in Fig. 2 and the details are examined in the previous study [27], the as-grown crystal by the Bridgman method was predominately composed of γ-phase with the fcc structure, but small amount of ε-phase with the hcp structure was contained. It is well known that the precipitated ε-phase often exhibits a strict crystal orientation relationship with respect to the γ-matrix-phase as follows:

$$\{111\}_\gamma // (0001)_\varepsilon, \quad <1\bar{1}0>_\gamma // <11\bar{2}0>_\varepsilon \tag{3}$$

Thus, four variant orientation relationships of (0001)//(111), $(\bar{1}11)$, $(1\bar{1}1)$ or $(11\bar{1})$ are geometrically considered for the precipitation of ε-phase; hereafter these variants are called ε_1, ε_2, ε_3 and ε_4, respectively. In the obtained single crystal, however, most of the ε-phase existed only on the plane parallel to (111), i.e., on the specific one of four {111} planes with a plate-like shape, as shown in Fig. 2. This is considered to be due to the relaxation of residual stress during the crystal growth process [27].

By the heat treatment of the single crystal, almost all of the γ-phases were transformed to ε-phase as shown in Fig. 10(b). Precipitation of other phases during the heat-treatment was not observed. Many of the formed ε-phases roughly satisfied the abovementioned crystal orientation relationship although large degree of deviation was observed in most cases, which can be understood by the comparison of the pole figures of $\{111\}_\gamma$ and $(0001)_\varepsilon$ as shown in Fig. 10(c). It must be emphasized here that as a notably different feature of the ε-phases compared to those in the as-grown crystal, four variants of ε-phases, i.e. the ε-phases in which (0001) is nearly parallel to (111), $(\bar{1}11)$, $(1\bar{1}1)$ or $(11\bar{1})$ were formed with an almost the same frequency in the annealed crystal. The shape of the ε-phase grains was not the plate-like but showed an indeterminate round shape. On the deformation mechanism of the ε-phase, we recently examined it by using the single crystal [28]. As a result, it was clarified that the (0001) basal slip and $\{10\bar{1}0\}$ prism slip are the predominate operative deformation modes. Their critical resolved shear stresses (CRSS) were estimated to be ~204 MPa for the basal slip and ~272 MPa for the prism slip, respectively. These values are much higher than that for {111}<112> slip which is the predominate deformation mode in the γ-phase (~54 MPa [27]). This large increase in CRSS by the phase transformation from the γ-phase to ε-phase must be the reason for the large increase in the hardness of the Co–Cr–Mo alloy by the heat-treatment, resulting in the increase in the wear resistance.

As shown in Fig. 6, the surface roughness on the worn pin was larger than that measured on the disk in the γ-phase. Since the disk contained ~30% of harder ε-phase, the γ-phase single crystalline pins were predominately reduced with respect to the disk during the wear test, as shown in Figs. 3 and 4. On the other hand, in the annealed (111) pin which is fully composed of ε-phase, the surface roughness on the worn pin was smaller than that on the disk.

The present results obviously demonstrate that the heat-treatment at 800 °C is suitable for improving the wear resistance via the fully phase transformation from γ-phase to ε-phase. However, the crystal orientation dependence of the wear behavior of the annealed specimen has not been clarified yet in the present state. As shown in Fig. 10, weak texture by hcp ε-phase is developed in the annealed specimen. Thus, the texture in the annealed specimen may be varied depending on the crystal orientation of the initial γ-phase, and it might affect the wear behavior. However, the details are not known yet. To clarify the orientation dependence of the wear behavior of hcp ε-phase is the next challenge by using the single crystal that we recently succeeded to fabricate [28].

4. Discussion

4.1. Origin of the orientation dependence of the hardness in the Co–Cr–Mo single crystal

To discuss the origin of the orientation dependence of the hardness, the relation between the Taylor factor is proposed by some researchers [42–44]. Formation of Vickers indentation requires the three-dimensional deformation of the material. To accomplish this, the satisfaction of Von Mises criterion is required, i.e. five independent slip systems are required for a material to undergo an arbitrarily imposed deformation. As a factor to evaluate the ease of such three-dimensional deformation, Taylor factor is proposed. The Taylor factor, M, is the coefficient to express the relation between the macroscopic stress σ and

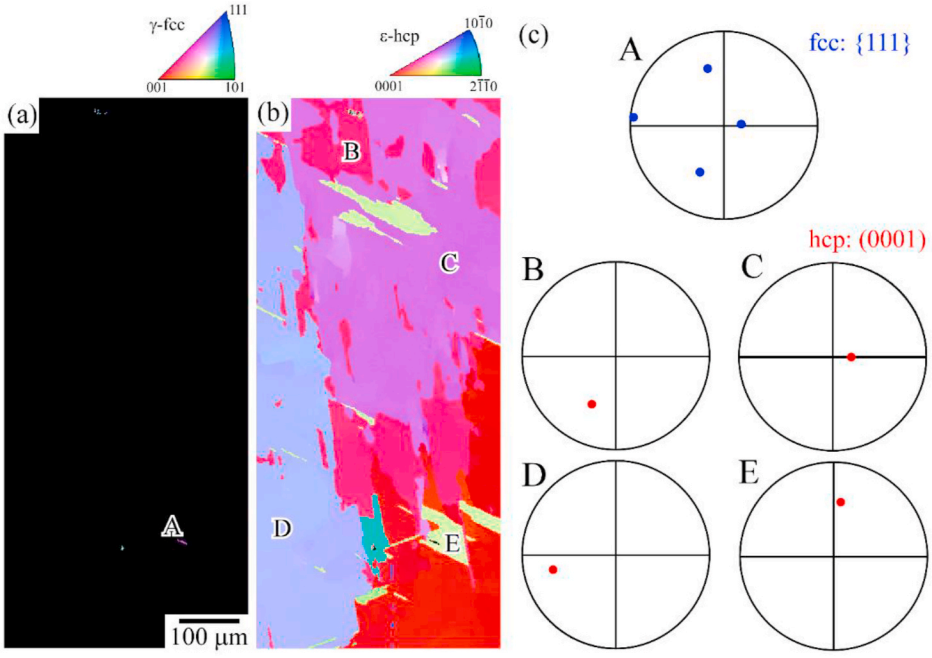

Fig. 10. (a, b) Crystal orientation maps taken in the heat-treated crystal at 800 °C for 40 h, for (a) fcc γ-phase and (b) hcp ε-phase. (c) {111} and (0001) pole figures measured at the positions A-E indicated in Fig. 10(a, b).

average microscopic shear stress $\bar{\tau}$ in the deformation of a material (polycrystal), as follows

$$\sigma = M \cdot \bar{\tau} \text{ and } \bar{\tau} = \frac{\sum \tau_s d\gamma_s}{\sum d\gamma_s} \quad (4)$$

where $d\gamma_s$ is the magnitude of the shear strain increment for slip system (deformation mode) s, and τ_s is the critical resolved shear stress for the deformation mode. Based on this relation (4), in a single crystal in which multiple slip systems are activated, the Taylor factor M can be defined as follows:

$$M = \frac{\sum_{s=1}^{5} d\gamma_s}{d\varepsilon} \quad (5)$$

where ε is the magnitude of the imposed strain increment [42,45]. The combination of five slip systems in the calculation is decided by solving for minimum value of M. From these expressions, it can be understood that the inverse of the M corresponds to a shear weighed average of the Schmid factors for multiple slip systems. The details of the evaluation method of the Taylor factor in a single crystal are described in Ref. [46]. The Taylor factor varies with the loading orientation in a single crystal, since the number of operative slip system and their Schmid factors vary depending on the loading axis. At the present state, however, the details on the orientation dependence of the Taylor factor in the Co–Cr–Mo single crystal has not been reported until now, since the predominately operative slip system in the γ Co–Cr–Mo alloy is not the {111}<101> slip as observed in general fcc crystals, but the {111}<112> slip is operative [27]. It has been reported that the motion of the <112> dislocation exhibit the asymmetry in tension and compression, since the formation of stacking fault accompanies behind the a/6<112> dislocation, and then it induces the development of ε-SIM [27,47]. Thus, the precise Taylor factor taking such asymmetry of the motion of <112> dislocation into consideration has not been evaluated yet. However, the variation tendency of the Taylor factor with loading orientation can be roughly anticipated by considering the Schmid factor of the operative {111}<112> slip. Table 2 shows the Schmid factors at the [001], [110] and [111] loading orientations for the twelve {111}<112> slip systems in which the asymmetric motion of them is also taken into consideration. The superscripts t and c indicate that they can be operative under tensile and compressive stress, respectively. It can be understood that in the compressive deformation along [111], six slip systems can be operative. While in deformation along [001] and [110], only four slip systems can be operative in compression, as schematically shown in Fig. 11. As described above, operation of five independent slip systems are required for the three-dimensional deformation in the Von Mises criterion. Thus, the Taylor factor at [111] orientation is expected to be lower than those at [001] and [110] orientations, and this may be related to the reason that the hardness on (001) and (110) is higher than that on (111). In addition, when compared the absolute value of the Schmid factor on (001) and (110), the average value is smaller on (110) than (001). Such differences in the number of operative deformation mode and their Schmid factors depending on the loading orientation must be related to the variation in hardness. More study using the computational simulation is required to discuss the further details on this.

Table 2
Schmid factors for the possible {111}<112> slips (ε-SIM formation) in the γ-phase single crystal at [001], [110], and [111] loading orientations. The superscript t and c indicate the ε-SIMs which are expected to form under the tensile and compressive deformation, respectively.

	[001]	[110]	[111]
(111)a/6[$\bar{1}\bar{1}$2]	0.471^{c}	0.471^{t}	0.000
(111)a/6[$\bar{1}$2$\bar{1}$]	0.236^{t}	0.236^{c}	0.000
(111)a/6[2$\bar{1}\bar{1}$]	0.236^{t}	0.236^{c}	0.000
($\bar{1}$11)a/6[1$\bar{1}$2]	0.471^{c}	0.000	0.157^{c}
($\bar{1}$11)a/6[12$\bar{1}$]	0.236^{t}	0.000	0.157^{c}
($\bar{1}$11)a/6[2$\bar{1}\bar{1}$]	0.236^{t}	0.000	0.314^{t}
(1$\bar{1}$1)a/6[$\bar{1}$12]	0.471^{c}	0.000	0.157^{c}
(1$\bar{1}$1)a/6[$\bar{1}$2$\bar{1}$]	0.236^{t}	0.000	0.314^{t}
(1$\bar{1}$1)a/6[21$\bar{1}$]	0.236^{t}	0.000	0.157^{c}
($\bar{1}\bar{1}$1)a/6[112]	0.471^{c}	0.471^{t}	0.314^{t}
($\bar{1}\bar{1}$1)a/6[1$\bar{2}$1]	0.236^{t}	0.236^{c}	0.157^{c}
($\bar{1}\bar{1}$1)a/6[$\bar{2}$11]	0.236^{t}	0.236^{c}	0.157^{c}

4.2. Formation of ε-SIM that affects the orientation dependence of the wear behavior

It was found in this study that the wear behavior of the Co–Cr–Mo single crystal shows relatively strong orientation dependence; the wear resistance is higher in order of (110) > (001) > (111). One of the reasons for this behavior is that the hardness shows the orientation dependence with the same tendency as that of the wear resistance, as clarified in Fig. 9(b). In addition to this, we found that the developing feature of the deformation microstructure during the wear test was different depending on the loading orientation. In this section, the origin of the orientation dependence of the wear behavior of the Co–Cr–Mo single crystal is further discussed on the basis of the variation in the deformation microstructure.

Fig. 12(a–f) show the crystal orientation maps at the tip of the worn pin after the test for 1 week. At the tip of the pin, formation of ε-phases driven by the wear deformation was confirmed in all the specimens. Among the four variants, the ε_1 variant with the interface parallel to (111) and parallel to the grown-in variant was significantly developed compared to other three variants in all the specimens. This is owing to the difficulty of the growth of the other variants beyond the pre-existing variants during the development of ε-SIMs, as clarified in a previous study in the monotonic compression test [27]. It is to note here that the volume fraction of the formed ε_1 variant was obviously different depending on the loading orientation; the volume fraction was larger in order of (110) > (001) > (111). More precisely, the area fraction of ε-phase measured by SEM-EBSD at around the region shown in Fig. 12 was ~98%, ~40% and ~10% in the (110), (001), and (111) pin, respectively. Especially in the (110) specimen, the almost entire surface was covered by the transformed ε-phase. This was further confirmed by the observation used transmission electron microscopy (TEM) as shown in Fig. 13. The selected area electron diffraction (SAED) pattern indicates that the surface of the worn specimen was almost entirely covered by the ε-phase (Fig. 13(a)), but the volume fraction of the ε-phase was drastically decreased at the position ~200 μm away from the worn surface (Fig. 13(b)). This demonstrates that the localized deformation during the wear test induced the formation of ε-SIM at the tip of the worn pin. As shown in Fig. 13(a), in the ε-phase formed at the tip part, many amounts of dislocations were introduced by further deformation.

Interestingly, the volume fraction of ε-SIM induced by the wear in each specimen shows a strong correlation with the order of wear resistance shown in Fig. 3, i.e. in the specimen with larger volume fraction of ε-SIM, the smaller wear volume was measured. As clarified by the wear test of the heat-treated single crystal, the formation of ε-phase increases the wear resistance owing to its higher hardness. Thus, the formability of the strain-induced ε-SIM during the wear test also must affect the orientation dependence of the wear resistance of the γ-phase crystal. The variation in formability of the ε-SIMs is expected to be anticipated by considering their Schmid factor in the wear test. Here, it must be mentioned that the stress applied direction in the pin, which affects the formation behavior of the ε-SIM, is not simply parallel to the pin during the wear test, but it must be along the direction as the summation of the

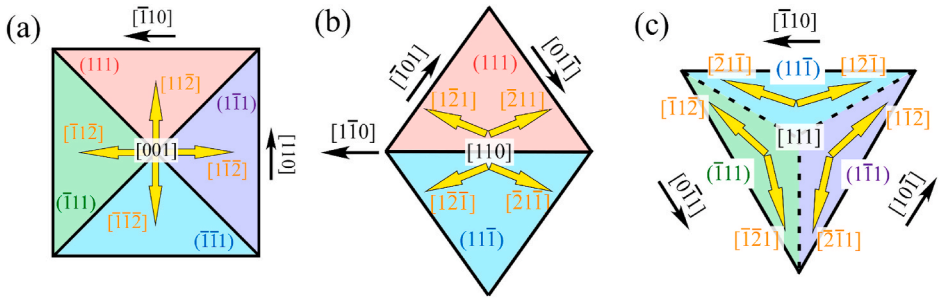

Fig. 11. Schematics showing the operative {111}a/6<112> slip systems for deformations along (a) [001], (b) [110] and (c) [111] in compression.

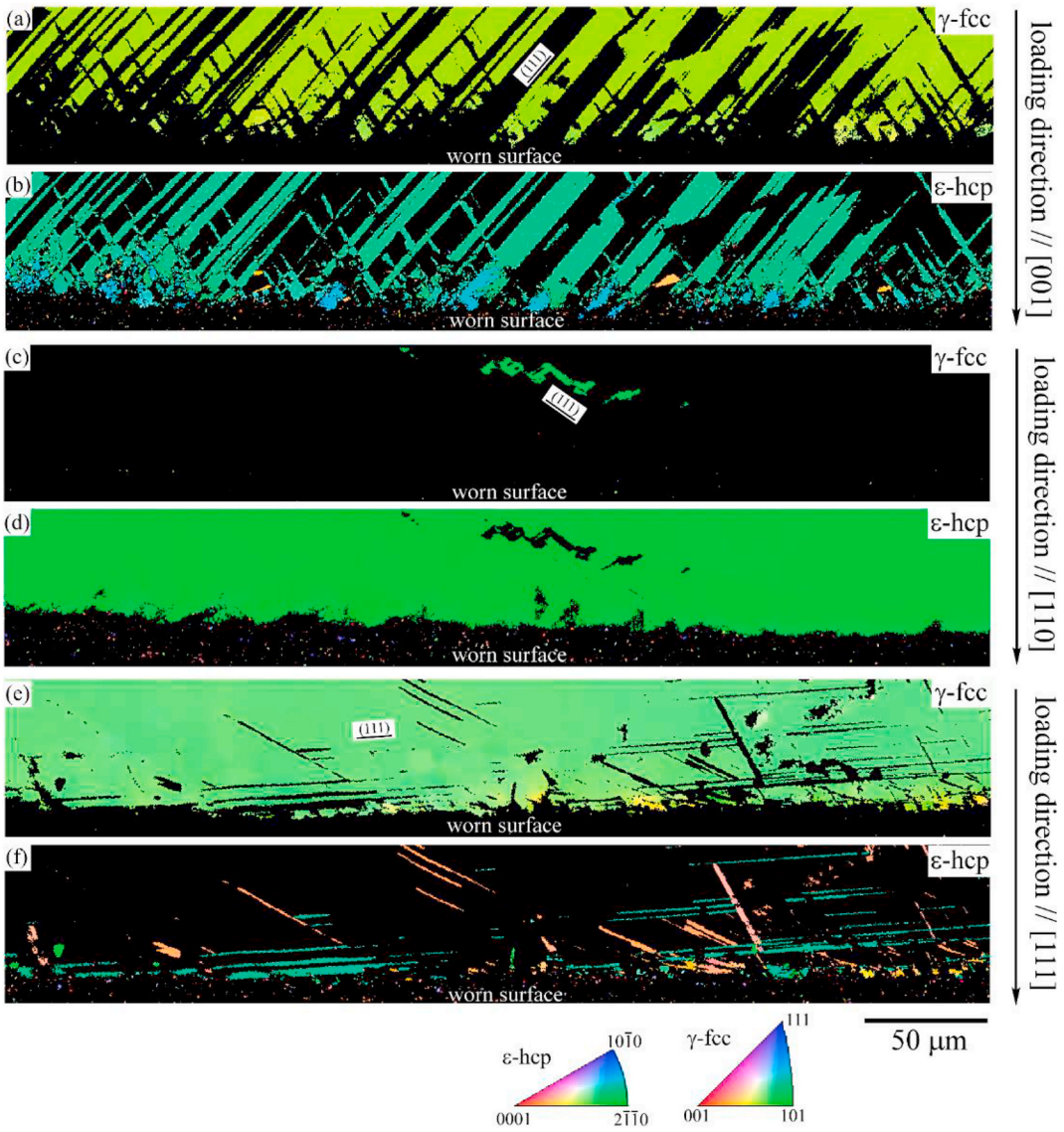

Fig. 12. Crystal orientation maps taken at the tip of the worn single crystalline pins after the wear test for 1 week. (a,b) [001], (c,d) [110] and (e,f) [111] specimens. Observed direction is roughly close to [1$\bar{1}$0] shear direction in the wear test in all the figures.

normal loading stress, N, and the friction shear stress generated by wear, μN. Here, the coefficient of friction μ was evaluated to be ~0.44–0.46 in the present experiment, as shown in Fig. 6. Thus, assuming that μ = 0.45, the effective stress direction applied to the pin during the wear test can be estimated. Table 3 indicates the Schmid factors for {111}<112> slips along the resultant stress direction with the loading stress and the friction shear stress. Among the slip systems listed in Table 3, the slip on (111) is preferentially operative as described above. When compared to the largest Schmid factor for the slip on (111), the value was larger in the specimens in order of (110) > (001) > (111). This is in good agreement with the order of evaluated volume fraction of the formed ε_1-variant and the wear resistance.

In Fig. 3, the wear volume was almost proportionally increased with the sliding distance throughout the test in (001) and (111) specimens.

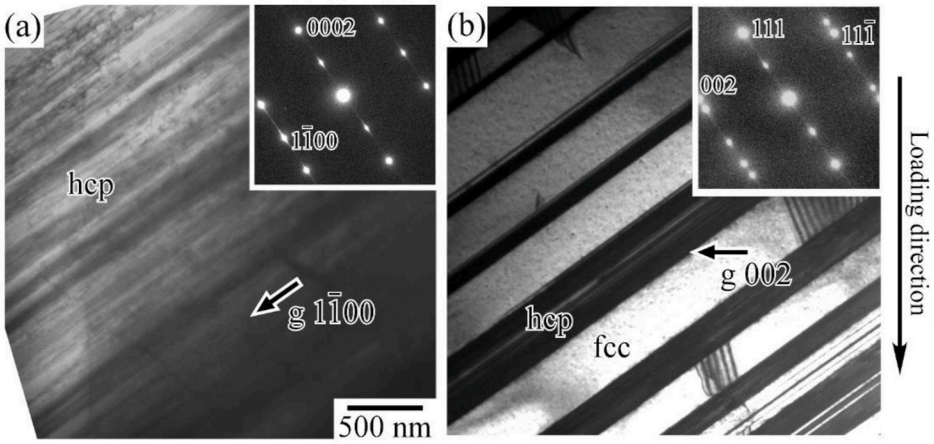

Fig. 13. TEM bright field images showing the deformation microstructure in the worn pin with the loading orientation parallel to [110], observed along [$\bar{1}$10]. The observed positions are (a) just beneath the worn surface, (b) ~200 μm away from the worn surface, respectively.

Table 3
Schmid factors for the possible {111}<112> slips (ε-SIM formation) in the γ-phase single crystal during the wear test, taking the influence of the friction stress into consideration.

Loading orientation	[001]	[110]	[111]
resultant stress direction	[$\bar{8}$ 8 25]	[11 29 0]	[9 31 20]
(111)a/6[$\bar{1}\bar{1}$2]	0.391[c]	0.392[t]	0.000
(111)a/6[$\bar{1}$2$\bar{1}$]	0.008[t]	0.461[c]	0.324[c]
(111)a/6[2$\bar{1}\bar{1}$]	0.383[t]	0.069[t]	0.324[t]
($\bar{1}$11)a/6[1$\bar{1}$2]	0.436[c]	0.079[t]	0.124[c]
($\bar{1}$11)a/6[12$\bar{1}$]	0.218[t]	0.304[c]	0.350[c]
($\bar{1}$11)a/6[2$\bar{1}\bar{1}$]	0.218[t]	0.225[t]	0.474[t]
(1$\bar{1}$1)a/6[$\bar{1}$12]	0.186[c]	0.079[t]	0.002[t]
(1$\bar{1}$1)a/6[$\bar{1}$2$\bar{1}$]	0.093[t]	0.304[c]	0.030[t]
(1$\bar{1}$1)a/6[21$\bar{1}$]	0.093[t]	0.225[t]	0.009[t]
($\bar{1}\bar{1}$1)a/6[112]	0.391[c]	0.392[t]	0.262[t]
($\bar{1}\bar{1}$1)a/6[1$\bar{2}$1]	0.383[t]	0.461[c]	0.239[c]
($\bar{1}\bar{1}$1)a/6[$\bar{2}$1$\bar{1}$]	0.008[t]	0.069[t]	0.023[c]

This feature is similar to that in the previous study used polycrystalline Co–Cr–Mo alloys by Saldívar-García and López [48]. On the other hand, the wear rate was slightly deceased at the latter period of the wear test in the (110) specimen, compared to those in the (111) and (001) specimens. This strongly suggests that the development of ε-SIM on the surface significantly decreases the wear rate at the latter period of the wear test in the (110) specimen. Further study is required to clearly establish this conclusion.

Regarding the abrasive wear resistance of the metallic materials, the f_{ab}-concept is proposed by Zum Gahr [49], where f_{ab} is defined as follows:

$$f_{ab} = \frac{A_v - (A_1 + A_2)}{A_v} \quad (6)$$

where A_v is the area of a wear groove measured on the cross-section through the groove and (A_1+A_2) are the areas of the materials pushed by plastic deformation to the groove edges. From the definition, ideal microploughing results in $f_{ab} = 0$ and ideal microcutting in $f_{ab} = 1$ [49]. Here, Zum Gahr described that the abrasive wear resistance is affected not only by hardness, but it also increased by increasing the capability of plastic deformation. And the capability of plastic deformation is influenced by work-hardening, strain distribution, mechanical instability etc. [49]. Relating to this point, the material which has low stacking-fault energy tends to show lower wear resistance, as it is experimentally examined by Schell et al. [50]. They clarified that abrasive wear resistance of pure-Ni shows higher wear resistance than that of Cu–30Ni alloy even though they have the same hardness. In them, f_{ab} in Ni shows smaller value than that in Cu–30Ni. This is because the inhomogeneous slip is induced in Cu–30Ni with low stacking fault energy, by the collective and planar motion of dislocations accompanied by the wide-distance of dislocation dissociation. This results in the increase in f_{ab} value and lead to the low wear resistance. This must be applicable to this study. The Co–Cr alloy has extremely low stacking fault energy [51], and thus the ε-SIM formation is induced during the wear, as confirmed in this study. Consequently, homogeneous work-hardening is difficult to occur on the surface. As shown in Fig. 12(e, f), the inhomogeneous deformation microstructure is typically developed in the (111) pin in which the Schmid factor for ε-SIM formation is small, even after long-time wear. The inhomogeneity of the strain distribution is expected to induce the increase in f_{ab} value, resulting in lower wear resistance. On the other hand, in the (110) pin, the ε-SIM fully covered the surface during the wear test as shown in Fig. 12(c, d). In the (110) pin, further deformation of the ε-phase is carried by the dislocation motion, as confirmed in Fig. 13(a). Thus, homogeneous work-hardening can occur on the surface, resulting in the increase in the wear resistance. The results strongly suggest that not only the hardness, but the distribution control of the ε-SIM is important to control the wear behavior of the Co–Cr alloys with the extremely low stacking fault energy, and it can be achieved by the crystal orientation control in the γ-phase.

From the results, further improvement of the wear resistance of the Co–Cr–Mo implant alloys is promising via the appropriate control of the crystal orientation (texture) and microstructure. This could contribute for the increase of the lifetime of Co–Cr–Mo implant alloys as well as patient healthcare and comfort. Moreover, the results give important information for the design of the novel "single-crystalline" artificial joints with much superior properties.

In this study, the wear test was conducted under the dry condition to clarify the intrinsic origin of the orientation dependence of the wear behavior. However, for the development of single-crystalline implant, the wear behavior under wet conditions, such as under simulated body fluids, also must be examined. It is currently being prepared by our group. The results will be reported in future.

5. Conclusions

In this study, the orientation dependence of the wear behavior of Co–Cr–Mo alloy for biomedical application was clarified by using the single crystal. The obtained results are summarized as follows.

(1) The wear resistance of the γ(fcc)-phase shows a strong orientation dependence. The wear resistance was higher on the planes in order of (110), (001) and (111). Quantitatively, the wear volume on (110) was more than 30% smaller than that on (111).
(2) The phase transformation from fcc to hcp structure induced by heat treatment largely increased the wear resistance.
(3) The variations in wear resistance showed qualitatively in good agreement with the variations in Vickers hardness of the specimens.
(4) In addition to the intrinsic orientation dependence of the hardness in the fcc-phase, the formation behavior of the deformation induced hcp-phase martensites, which varies depending on the loading orientation, strongly affects the wear resistance of the fcc Co–Cr–Mo alloy.

Data availability

The raw/processed data required to reproduce these findings cannot be shared at this time as the data also forms part of an ongoing study.

Declaration of competing interest

The authors declare that they have no known competing financial interests or personal relationships that could have appeared to influence the work reported in this paper.

Acknowledgements

This work was supported by Grants-in-Aid for Scientific Research from the Japan Society for the Promotion of Science (JSPS) [grant numbers: JP18H05254, JP20K21087, JP18H05478].

References

[1] A. Buford, T. Goswami, Review of wear mechanisms in hip implants Paper I – General, Mater. Des. 25 (2004) 385–393.
[2] A. Chiba, K. Kumagai, N. Nomura, S. Miyakawa, Pin-on-disk wear behavior in a like-on-like configuration in a biological environment of high carbon cast and low carbon forged Co–29Cr–6Mo alloys, Acta Mater. 55 (2007) 1309–1318.
[3] Y. Liao, R. Pourzal, P. Stemmer, M.A. Wimmer, J.J. Jacobs, A. Fischer, L.D. Marks, New insights into hard phases of CoCrMo metal-on-metal hip replacements, J. Mech. Behav. Biomed. 12 (2012) 39–49.
[4] D.M. Vasconcelos, S.G. Santos, M. Lamghari, M.A. Barbosa, The two faces of metal ions: from implants rejection to tissue repair/regeneration, Biomaterials 84 (2016) 262–275.
[5] E. Gibon, D.F. Amanatullah, F. Loi, J. Pajarinen, A. Nabeshima, Z. Yao, M. Hamadouche, S.B. Goodman, The biological response to orthopaedic implants for joint replacement: Part I: Metals, J. Biomed. Mater. Res. B Appl. Biomater. 105B (2017) 2162–2173.
[6] G.M. Keegan, I.D. Learmonth, C.P. Case, Orthopaedic metals and their potential toxicity in the arthroplasty patient: a review of current knowledge and future strategies, J. Bone Joint Surg. Br. 89 (2007) 567–573.
[7] H. Pandit, M. Vlychou, D. Whitwell, D. Crook, R. Luqmani, S. Ostlere, D.M. Murray, N.A. Athanasou, Necrotic granulomatous pseudotumours in bilateral resurfacing hip arthoplasties: evidence for a type IV immune response, Virchows Arch. 453 (2008) 529–534.
[8] I. Polyzois, D. Nikolopoulos, I. Michos, E. Patsouris, S. Theocharis, Local and systemic toxicity of nanoscale debris particles in total hip arthroplasty, J. Appl. Toxicol. 32 (2012) 255–269.
[9] D.C. Mears, Metals in medicine and surgery, Int. Met. Rev. 22 (1977) 119–155.
[10] A.J. Dempsey, R.M. Pilliar, G.C. Weatherly, T. Kilner, The effects of nitrogen additions to a cobalt-chromium surgical implant alloy Part 2 Mechanical properties, J. Mater. Sci. 22 (1987) 575–581.
[11] A. Salinas-Rodriguez, J.L. Rodriguez-Galicia, Deformation behavior of low-carbon Co-Cr-Mo alloys for low-friction implant applications, J. Biomed. Mater. Res. 31 (1996) 409–419.
[12] P. Huang, H.F. Lopez, Strain induced ε-martensite in a Co–Cr–Mo alloy grain size effects, Mater. Lett. 39 (1999) 244–248.
[13] K. Yamanaka, M. Mori, S. Kurosu, H. Matsumoto, A. Chiba, Ultrafine grain refinement of biomedical Co-29Cr-6Mo alloy during conventional hot-compression deformation, Metall. Mater. Trans. 40A (2009) 1980–1994.
[14] M. Mori, K. Yamanaka, H. Matsumoto, A. Chiba, Evolution of cold-rolled microstructures of biomedical Co–Cr–Mo alloys with and without N doping, Mater. Sci. Eng. A 528 (2010) 614–621.
[15] A. Mani, Salinas-Rodriguez, H.F. Lopez, Deformation induced FCC to HCP transformation in a Co–27Cr–5Mo–0.05C alloy, Mater. Sci. Eng. A 528 (2011) 3037–3043.
[16] Y. Koizumi, S. Suzuki, K. Yamanaka, B.-S. Lee, K. Sato, Y. Li, S. Kurosu, H. Matsumoto, A. Chiba, Strain-induced martensitic transformation near twin boundaries in a biomedical Co–Cr–Mo alloy with negative stacking fault energy, Acta Mater. 61 (2013) 1648–1661.
[17] J.L. Tipper, P.J. Firkins, E. Ingham, J. Fisher, M.H. Stone, R. Farrar, Quantitative analysis of the wear and wear debris from low and high carbon content cobalt chrome alloys used in metal on metal total hip replacements, J. Mater. Sci. Mater. Med. 10 (1999) 353–362.
[18] J. Cawley, J.E.P. Metcalf, A.H. Jones, T.J. Band, D.S. Skupien, A tribological study of cobalt chromium molybdenum alloys used in metal-on-metal resurfacing hip arthroplasty, Wear 255 (2003) 999–1006.
[19] N. Maruyama, H. Kawasaki, A. Yamamoto, S. Hiromoto, H. Imai, T. Hanawa, Friction-wear properties of nickel-free Co–Cr–Mo alloy in a simulated body fluid, Mater. Trans. 46 (2005) 1588–1592.
[20] K. Kumagai, N. Nomura, T. Ono, M. Hotta, A. Chiba, Dry friction and wear behavior of forged Co–29Cr–6Mo alloy without Ni and C Additions for Implant Applications, Mater. Trans. 46 (2005) 1578–1587.
[21] L.C. Julián, A.I. Munöz, Influence of microstructure of HC CoCrMo biomedical alloys on the corrosion and wear behaviour in simulated body fluids, Tribol. Int. 44 (2011) 318–329.
[22] C.G. Figueiredo-Pina, A.A.M. Neves, B.M.B. Neves, Corrosion-wear evaluation of a UHMWPE/Co–Cr couple in sliding contact under relatively low contact stress in physiological saline solution, Wear 271 (2011) 665–670.
[23] R. Pourzal, I. Catelas, R. Theissmann, C. Kaddick, A. Fischer, Characterization of wear particles generated from CoCrMo alloy under sliding wear conditions, Wear 271 (2011) 1658–1666.
[24] H. Zhang, L.-G. Qin, M. Hua, G.-N. Dong, K.-S. Chin, A tribological study of the petaloid surface texturing for Co-Cr-Mo alloy artificial joints, Appl. Sur. Sci. 332 (2015) 557–564.
[25] F. Ren, W. Zhu, K. Chu, Fabrication, tribological and corrosion behaviors of ultra-fine grained Co-28Cr-6Mo alloy for biomedical applications, J. Mech. Beh. Biomed. Mater. 60 (2016) 139–147.
[26] F.Z. Hassani, M. Ketabchi, S. Bruschi, A. Ghiotti, Effects of carbide precipitation on the microstructural and tribological properties of Co–Cr–Mo–C medical implants after thermal treatment, J. Mater. Sci. 51 (2016) 4495–4508.
[27] K. Hagihara, T. Nakano, K. Sasaki, Anomalous strengthening behavior of Co–Cr–Mo alloy single crystals for biomedical applications, Scripta Mater. 123 (2016) 149–153.
[28] W. Kaita, K. Hagihara, L.A. Rocha, T. Nakano, Plastic deformation mechanisms of biomedical Co–Cr–Mo alloy single crystals with hexagonal close-packed structure, Scripta Mater. 142 (2018) 111–115.
[29] K.P. Gupta, The Co-Cr-Mo (Cobalt-Chromium-Molybdenum) system, J. Phase Equilibria Diffus. 26 (2005) 87–92.
[30] R.D. Arnell, Frictional deformation of cobalt single crystals by high angle diamond indenters, Wear 38 (1976) 361–370.
[31] Y. Ohno, J. Inotani, Y. Kaneko, S. Hashimoto, Orientation dependence of high-angle grain boundary formation during sliding wear in copper single crystals, J. Japan Inst. Metals 74 (2010) 384–391 (in Japanese).
[32] S.Y. Tarasov, D.V. Lychagin, A.V. Chumaevskii, Orientation dependence of subsurface deformation in dry sliding wear of Cu single crystals, Appl. Sur. Sci. 274 (2013) 22–26.
[33] X. Meng, C. Fang, K. Niu, Tribological behavior anisotropy in sliding interaction of asperities on single-crystal Λ-iron: a quasi-continuum study, Tribol. Int. 118 (2018) 347–359.
[34] S.-H. Lee, K. Hagihara, T. Nakano, Microstructural and orientation dependence of the plastic deformation behavior in β-type Ti-15Mo-5Zr-3Al alloy single crystals, Metall. Mater. Trans. 43 (2012) 1588–1597.
[35] S.-H. Lee, M. Todai, M. Tane, K. Hagihara, H. Nakajima, T. Nakano, Biocompatible low Young's modulus achieved by Strong crystallographic elastic anisotropy in Ti-15Mo-5Zr-3Al alloy single crystal, J. Mech. Beh. Biomed. Mater. 14 (2012) 48–54.
[36] K. Hagihara, T. Nakano, H. Maki, Y. Umakoshi, M. Niinomi, Isotropic plasticity of β-type Ti-29Nb-13Ta-4.6Zr alloy single crystals for the development of single crystalline β-Ti implants, Sci. Rep. 6 (2016) 20779.
[37] K. Hagihara, T. Nakano, Experimental clarification of the cyclic deformation mechanisms of β-type Ti–Nb–Ta–Zr-alloy single crystals developed for the single-crystalline implant, Int. J. Plast. 98 (2017) 27–44.
[38] K. Hagihara, T. Nakano, M. Todai, Unusual dynamic precipitation softening induced by dislocation glide in biomedical beta-titanium alloys, Sci. Rep. 7 (2017) 8056.
[39] T.H.C. Childs, The sliding wear mechanisms of metals, mainly steels, Tribol. Int. 13 (1980) 285–293.
[40] T.O. Mulhearn, L.E. Samuels, The abrasion of metals: a model of the process, Wear 5 (1962) 478–498.
[41] K. Hokkirigawa, K. Kato, Z.Z. Li, The effect of hardness on the transition of the abrasive wear mechanism of steels, Wear 123 (1988) 241–251.
[42] S.F. Castro, J. Gallego, F.J.G. Landgraf, H.-J. Kestenbach, Orientation dependence of stored energy of cold work in semi-processed electrical steels after temper rolling, Mater. Sci. Eng. A 427 (2006) 301–305.
[43] T. Miura, K. Fujii, K. Fukuya, K. Takashima, Influence of crystal orientation on hardness and nanoindentation deformation in ion-irradiated stainless steels, J. Nucl. Mater. 417 (2011) 984–987.
[44] M. Hayakawa, K. Tomatsu, E. Nakayama, K. Okamura, M. Yamamoto, K. Shizawa, Evaluating microscopic hardness in ferritic steel based on crystallographic

measurements via electron backscatter diffraction, Mater. Sci. Eng. A 700 (2017) 281–290.
[45] G.Y. Chin, W.L. Mammel, Computer solutions of the Taylor analysis for axisymmetric flow, Trans. Met. Soc. AIME 239 (1967) 1400–1405.
[46] J.M. Rosenberg, H.R. Piehler, Calculation of the Taylor factor and lattice rotations for bcc metals deforming by pencil glide, Metall. Trans. 2 (1971) 257–259.
[47] A. Sato, Y. Sunaga, T. Mori, Contribution of the γ→ε transformation to the plastic deformation of stainless steel single crystals, Acta Metall. 25 (1977) 627–634.
[48] A.J. Saldívar-García, H.F. López, Microstructural effects on the wear resistance of wrought and as-cast Co-Cr-Mo-C implant alloys, J. Biomed. Mater. Res. 74 (2005) 269–274.
[49] Microstructure and wear of materials, in: K.H. Zum Gahr (Ed.), Tribology Series 10, Elsevier, 1987.
[50] J. Schell, P. Heilmann, D.A. Rigney, Friction and wear of Cu-Ni alloys, in: S. K. Rhee, et al. (Eds.), Wear of Materials, ASME, 1981, pp. 53–62.
[51] L.-Y. Ti, R. Lizárraga, H. Larsson, E. Holmström, L. Vitos, A first principles study of the stacking fault energies for fcc Co-based binary alloys, Acta Meter 136 (2017) 215–223.